Published for SISSA by Springer

Received: *April 30, 2021*
Accepted: *July 18, 2021*
Published: *August 16, 2021*

Shedding light on dark matter with recent muon (g − 2) and Higgs exotic decay measurements

Chih-Ting Lu,[a] **Raymundo Ramos**[b] **and Yue-Lin Sming Tsai**[c]

[a] *School of Physics, KIAS,*
85 Hoegiro, Dongdaemun-gu, Seoul 02455, Republic of Korea
[b] *Institute of Physics, Academia Sinica,*
Nangang, Taipei 11529, Taiwan
[c] *Key Laboratory of Dark Matter and Space Astronomy,*
Purple Mountain Observatory, Chinese Academy of Sciences, Nanjing 210008, China
E-mail: timluyu@kias.re.kr, raramos@gate.sinica.edu.tw, smingtsai@pmo.ac.cn

Abstract: Recently, we have witnessed two hints of physics beyond the standard model: a 3.3σ local excess ($M_{A_0} = 52\,\text{GeV}$) in the search for $H_0 \to A_0 A_0 \to b\bar{b}\mu^+\mu^-$ and a 4.2σ deviation from the SM prediction in the $(g-2)_\mu$ measurement. The first excess was found by the ATLAS collaboration using $139\,\text{fb}^{-1}$ data at $\sqrt{s} = 13\,\text{TeV}$. The second deviation is a combination of the results from the Brookhaven E821 and the recently reported Fermilab E989 experiment. We attempt to explain these deviations in terms of a renormalizable simplified dark matter model. Inspired by the null signal result from dark matter (DM) direct detection, we interpret the possible new particle, A_0, as a pseudoscalar mediator connecting DM and the standard model. On the other hand, a new vector-like muon lepton can explain these two excesses at the same time while contributing to the DM phenomenology.

Keywords: Beyond Standard Model, Higgs Physics

ArXiv ePrint: 2104.04503

https://doi.org/10.1007/JHEP08(2021)073

JHEP08(2021)073

Contents

JHEP08(2021)073

1 Introduction

The existence of dark matter (DM) is now well established by old and new astrophysical and cosmological evidence. Conversely, its particle properties remain unclear, in particular, the way to incorporate DM and its interactions into the standard model (SM) of particle physics. In the case of DM-quark interaction, current DM direct detection experiments, such as XENON1T, have not observed any DM-nuclei scattering evidence [1]. Furthermore, the Muon $g-2$ collaboration at Fermilab has recently reported an eye-catching measurement of the anomalous magnetic dipole moment of $\mu^\pm$ with a 3.3σ deviation from the SM prediction achieving a combined experimental average of $\Delta a_\mu = (2.51 \pm 0.59) \times 10^{-9}$ [2]. This confirms a long standing tension between SM and experimental data that was previously reported by the E821 experiment at Brookhaven National Laboratory, inspiring several beyond the SM (BSM) extensions (see ref. [3] for a review). The new average is consistent with a 4.2σ deviation from the SM prediction strongly motivating new proposals [4–52]. Furthermore, the ATLAS collaboration has reported a search for the Higgs boson exotic decay channel $H_0 \to A_0 A_0 \to b\bar{b}\mu^+\mu^-$, using $139\,\text{fb}^{-1}$ data at $\sqrt{s} = 13\,\text{TeV}$ [53].

They have taken the muon pair as a trigger to search for the narrow dimuon resonance of a light spin-0 particle A_0. A deviation from the SM background with a local (global) significance of 3.3σ (1.7σ) is reported at $M_{A_0} = 52\,\text{GeV}$ with the branching fraction given by $\text{BR}(H_0 \to A_0 A_0 \to b\bar{b}\mu^+\mu^-) \sim 3.5\times10^{-4}$. Therefore, the null observation from XENON1T and the two possible BSM observations (Δa_μ and $H_0 \to A_0 A_0 \to b\bar{b}\mu^+\mu^-$) can be interpreted as hints that the new spin-0 particle A_0 can serve as a mediator to connect DM with SM, especially for its non-trivial coupling with muons.

One can simply consider the additional spin-0 particle A_0 coupling to SM fermion pairs via the mixing with SM-like Higgs boson only or like the scalar/pseudoscalar in the conventional two Higgs doublet models (Type-I, II, X, and Y 2HDM [54], 2HDM+S [55]) with $M_{A_0} = 52\,\text{GeV}$. However, their predicted signal strength for $\text{BR}(H_0 \to A_0 A_0 \to b\bar{b}\mu^+\mu^-)$ cannot reach the measured 3.5×10^{-4} when including all other experimental constraints [56, 57]. We go beyond the models mentioned above and involve a new vector-like muon lepton (VLML) not only to enhance $\text{BR}(A_0 \to \mu^+\mu^-)$ but also to contribute to Δa_μ [60], thus, explaining both excesses. Motivated by these observations and from theoretical considerations, we propose a renormalizable simplified DM model based on extending the SM with three SM singlet fields: a Dirac DM, a VLML, and a pseudoscalar mediator. One important advantage of adopting a pseudoscalar mediator here is that the elastic cross section of DM-nuclei collision is suppressed by the small recoil energy making easy to escape the current XENON1T stringent limit.

The paper is organized as follows. First, we briefly discuss the model setup in section 2. Next, we consider relevant constraints for this model used in our likelihood functions in section 3. In section 4, we present our numerical analysis and the 2σ allowed regions. Finally, we conclude in section 5.

2 Renormalizable simplified dark matter model

In this section, we show our model configuration. We consider a SM singlet Dirac fermion χ as a DM candidate. A new pseudoscalar mediator A is also introduced to explain the null signal result in DM direct detection and possible excess in Higgs exotic decay. Additionally, we introduce a VLML, $\psi^\pm$, that will contribute to the $(g-2)_\mu$ excess. Thus, the renormalizable Lagrangian for this simplified DM model can be written as

$$\begin{aligned}\mathcal{L} = \mathcal{L}_{\text{SM}} &+ \overline{\chi}(i\partial\!\!\!/ - M_\chi - ig_\chi A\gamma_5)\chi + \frac{1}{2}\partial_\mu A \partial^\mu A - \frac{1}{2}m_A^2 A^2 \\ &- (\mu_A A + \lambda_{HA} A^2)\left(H^\dagger H - \frac{v^2}{2}\right) - \frac{\mu'_A}{3!}A^3 - \frac{\lambda_A}{4!}A^4 \\ &+ \left[-\kappa\overline{L}_\mu H \psi_R + i\kappa'\overline{\mu}_R A\psi_L - iy\overline{\psi}_L A\psi_R + M_\psi\overline{\psi}_L\psi_R + \text{H.c.}\right]. \end{aligned} \tag{2.1}$$

where H is the SM scalar $\text{SU}(2)_L$ doublet and L_μ is the second generation left-handed lepton doublet. Note that the dimension-3 terms with μ_A and μ'_A break the parity [61]. The tadpole for A is removed and $\langle A\rangle = 0$ is assumed in this model.

After electroweak symmetry breaking (EWSB), the pseudoscalar A and the SM Higgs boson h mix with each other via the μ_A term. The relation between the mass eigenstates,

JHEP08(2021)073

H_0 and A_0, and the interaction states, h and A, is

$$\begin{pmatrix} H_0 \\ A_0 \end{pmatrix} = \begin{pmatrix} \cos\alpha & \sin\alpha \\ -\sin\alpha & \cos\alpha \end{pmatrix} \begin{pmatrix} h \\ A \end{pmatrix} \tag{2.2}$$

where the mixing angle, α, is given by

$$\sin 2\alpha = \frac{2\mu_A v}{M_{H_0}^2 - M_{A_0}^2} \tag{2.3}$$

with $v \sim 246\,\text{GeV}$ the vacuum expectation value. We assign H_0 as the SM-like Higgs boson with $M_{H_0} = 125\,\text{GeV}$ and A_0 with $M_{A_0} = 52\,\text{GeV}$ to explain the ATLAS Higgs boson exotic decay excess [53]. In the next section, we will see that the LHC Higgs boson measurements can put a strong upper limit on $\sin 2\alpha$ in this model. Similarly, the VLML and muon will mix together after EWSB [60]. According to $Z \to l^+ l^-$ precision measurements [62], an upper limit for the mixing between the left-handed muon and VLML is set at

$$\frac{\kappa v}{\sqrt{2} M_\psi} < \mathcal{O}(10^{-2}). \tag{2.4}$$

where $M_\psi \sim v$ implies $\kappa \lesssim \mathcal{O}(10^{-2})$. In contrast, κ' doesn't suffer from this constraint and its value can be larger.

The Lagrangian to describe the interactions between the SM sector and DM sector via H_0 and A_0 portal can be written as

$$\begin{aligned} \mathcal{L}_{\text{int}}^{(H_0,A_0)} = & -ig_\chi \left(H_0 s_\alpha + A_0 c_\alpha\right) \overline{\chi}\gamma_5\chi - \left(H_0 c_\alpha - A_0 s_\alpha\right) \left[\sum_{f\neq\mu} \frac{m_f}{v} \overline{f} f - \sum_{V=Z,W^\pm} \frac{\delta_V m_V^2}{v} V_\mu V^\mu\right] \\ & - \left(\frac{m_\mu}{v} c_\alpha + i g_A \gamma_5 s_\alpha\right) H_0 \overline{\mu}\mu + \left(\frac{m_\mu}{v} s_\alpha - i g_A \gamma_5 c_\alpha\right) A_0 \overline{\mu}\mu \end{aligned} \tag{2.5}$$

where $s_\alpha = \sin\alpha$, $c_\alpha = \cos\alpha$ and in the first-order approximation of κ,

$$g_A = \frac{\kappa'\kappa}{\sqrt{2}} \frac{v}{M_\psi} \tag{2.6}$$

and $\delta_V = 1(2)$ for $V = Z(W^\pm)$. Note that, excepting muon pair, there are only axial (scalar) couplings for H_0 and A_0 with DM pair (SM fermion pairs). The term with g_A is important to enhance $\text{BR}(A_0 \to \mu^+\mu^-)$. Additionally, the CP-violation effect in the muon Yukawa interactions is a feature of this model. For the first order of κ approximation, the interactions of VLML can be expanded as

$$\begin{aligned} \mathcal{L}_{\text{int}}^{\psi} = & -e\overline{\psi}\gamma^\mu\psi A_\mu + \frac{g}{c_W}\overline{\psi}\gamma^\mu\psi Z_\mu - iy\overline{\psi}(H_0 s_\alpha + A_0 c_\alpha)\gamma^5\psi \\ & + \Big[-\frac{\kappa}{\sqrt{2}}(H_0 c_\alpha - A_0 s_\alpha)\overline{\mu}_L\psi_R + i\kappa'(H_0 s_\alpha + A_0 c_\alpha)\overline{\mu}_R\psi_L \\ & + g_z'\overline{\mu}_L\gamma^\mu\psi_L Z_\mu + g_w'\overline{\nu}\gamma^\mu\psi_L W_\mu^+ + \text{H.c.}\Big] \end{aligned} \tag{2.7}$$

JHEP08(2021)073

where

$$g'_z = -\frac{g'_w}{\sqrt{2}c_W}, \quad g'_w = \frac{\kappa g}{2}\frac{v}{M_\psi}. \tag{2.8}$$

Note that the $\{H_0, A_0\}\mu\psi$ terms in eq. (2.7) can contribute to Δa_μ via one-loop Feynman diagrams [60].

From eq. (2.1) we can read off ten undetermined parameters in this model:

$$g_\chi, \quad s_\alpha, \quad M_\chi, \quad \lambda_{HA}, \quad \mu'_A, \quad \lambda_A, \quad \kappa, \quad \kappa', \quad y, \quad M_\psi. \tag{2.9}$$

We can further fix $\mu'_A = 5.0\,\text{GeV}$, $\lambda_A = 1.0$ and $y = 0.01$ for this analysis because their changes are neither relevant nor significant for this work. Considering that the LHC Higgs boson measurements constrain $\sin^2\alpha < 0.12$ at 95% C.L. [63, 64], we assign the upper bound $\sin\alpha < 0.3$ in our parameter scan.[1] As required by eq. (2.4), κ cannot be large and one has to introduce a larger κ' to explain the Δa_μ deviation. Furthermore, a very massive $\psi^\pm$ could suppress the contribution to Δa_μ when we require perturbativity of κ' with $\kappa' \leq \sqrt{4\pi}$. Finally, for simplicity, we assume $M_{A_0}/2 < M_\chi < M_\psi$ such that $A_0 \to \chi\overline{\chi}$ and the annihilation $\chi\overline{\chi} \to \psi^+\psi^-$ are kinematically forbidden. Taking all these facts into consideration, the scan range for the non-fixed parameters is given by the followings bounds

$$\begin{aligned}
10^{-3} &\leq g_\chi^{(*)} \leq 2.0\,, \\
5\times10^{-3} &\leq \sin\alpha^{(*)} \leq 0.3\,, \\
150.0 &\leq M_\psi/\text{GeV} \leq 450.0\,, \\
26.0 &\leq M_\chi/\text{GeV} \leq 0.9\times M_\psi/\text{GeV}\,, \\
5\times10^{-4} &\leq \lambda_{HA}^{(*)} \leq 10^{-2}\,, \\
3\times10^{-6} &\leq \kappa^{(*)} \leq 8\times10^{-2}\,, \\
1.0 &\leq \kappa' \leq \sqrt{4\pi}\,,
\end{aligned} \tag{2.10}$$

where the star $(*)$ indicates that the parameter is scanned logarithmically in base 10.

3 Experimental constraints

Recently, the Muon $g-2$ collaboration at Fermilab reported a new measurement of the anomalous magnetic dipole moment of the muon achieving the new combined result [2]

$$\Delta a_\mu = (2.51 \pm 0.59)\times10^{-9} \tag{3.1}$$

consistent with a 4.2σ deviation from the SM. Note that the SM uncertainties have been taken into account in the error bar.[2] The dominant BSM contributions to $(g-2)_\mu$ in this model comes from one-loop Feynman diagrams with $\psi^\pm$, A_0, and H_0 as [60]

$$\Delta a_\mu = \frac{\kappa'^2}{96\pi^2}\frac{m_\mu^2}{M_\psi^2}\left[c_\alpha^2 f\left(\frac{M_{A_0}^2}{M_\psi^2}\right) + s_\alpha^2 f\left(\frac{M_{H_0}^2}{M_\psi^2}\right)\right] \tag{3.2}$$

[1] We will see in the next section that constraints from Higgs boson invisible and exotic decays are much stronger than this limit in our model.

[2] The SM central value and error bar for $(g-2)_\mu$ use the theoretical consensus value with hadronic vacuum polarization (HVP) determined from $e^+e^- \to$ hadrons (see, for example, [58]). Note that a recent calculation for the HVP on the lattice finds no significant tension between measurement and SM prediction [59].

JHEP08(2021)073

where $f(t) = (2t^3 + 3t^2 - 6t^2 \ln t - 6t + 1)/(t-1)^4$. Because of the constraint in eq. (2.4) and large CP-violation effect of muon EDM, we can safely assume $\kappa \ll \kappa'$.

Furthermore, the ATLAS collaboration has detected a local excess in the Higgs decay channel $H_0 \to A_0 A_0 \to b\bar{b}\mu^+\mu^-$ at $M_{A_0} = 52\,\text{GeV}$, by using $139\,\text{fb}^{-1}$ data at $\sqrt{s} = 13\,\text{TeV}$ [53]. The measured branching ratio $\text{BR}(H_0 \to A_0 A_0 \to b\bar{b}\mu^+\mu^-)$ is around 3.5×10^{-4} with a local 3.3σ significance. By taking a conservative approach, we assume that the central value is located at 3.5×10^{-4} and the likelihood is a Gaussian distribution with error bar equal to 3.5×10^{-4} divided by 3.3 at $M_{A_0} = 52\,\text{GeV}$. In the on-shell limit, we can calculate $\text{BR}(H_0 \to A_0 A_0)$, $\text{BR}(A_0 \to b\bar{b})$ and $\text{BR}(A_0 \to \mu^+\mu^-)$ individually and then multiply them together to obtain $\text{BR}(H_0 \to A_0 A_0 \to b\bar{b}\mu^+\mu^-)$.

We can divide the major constraints used for this study in five categories: (1) the LHC Higgs boson measurements, (2) the LEP and LHC A_0 searches, (3) the DM phenomenology, (4) the ATLAS multi-lepton search and (5) electron, muon electric dipole moments (EDMs).

3.1 The LHC Higgs boson measurements

For the LHC Higgs boson measurements, one can further classify them as

- **Higgs boson exotic and invisible decays.**
  We take $\text{BR}(H_0 \to \text{undetected}) < 19\%$ and $\text{BR}(H_0 \to \text{invisible}) < 9\%$ at 95% C.L. as reported by ref. [57]. The partial decay width of $H_0 \to A_0 A_0$ can be written as

$$\Gamma(H_0 \to A_0 A_0) = \frac{\lambda^2_{H_0 A_0 A_0}}{32\pi M_{H_0}} \sqrt{1 - 4\left(\frac{M_{A_0}}{M_{H_0}}\right)^2} \tag{3.3}$$

  where

$$\lambda_{H_0 A_0 A_0} = -\mu_A s^3_\alpha - 2(3\lambda_H - 2\lambda_{HA}) v s^2_\alpha c_\alpha - 2\lambda_{HA} v c^3_\alpha + (2\mu_A - \mu'_A) s_\alpha c^2_\alpha. \tag{3.4}$$

  If $m_\chi < M_{H_0}/2$, the Higgs boson can also decay to a pair of DM as

$$\Gamma(H_0 \to \chi\overline{\chi}) = s^2_\alpha g^2_\chi \frac{M_{H_0}}{8\pi} \left(1 - \frac{4m^2_\chi}{M^2_{H_0}}\right)^{3/2}. \tag{3.5}$$

  Therefore, we require

$$\begin{aligned} \text{BR}(H_0 \to A_0 A_0) + \text{BR}(H_0 \to \chi\overline{\chi}) &< 19\%, \text{and} \\ \text{BR}(H_0 \to \chi\overline{\chi}) &< 9\%. \end{aligned} \tag{3.6}$$

  Note that, in this study, we fix $M_{A_0} = 52\,\text{GeV}$ such that $\Gamma(H_0 \to A_0 A_0)$ is a function of $\sin\alpha$ and λ_{HA} only.

- $\boldsymbol{H_0 \to \mu^+\mu^-}$**.**
  The decay width $\Gamma(H_0 \to \mu^+\mu^-)$ can be modified by changing the μ–ψ mixing. We require the measured signal strength of $H_0 \to \mu^+\mu^-$, relative to the SM prediction, to be $1.19^{+0.44}_{-0.42}(\text{stat})^{+0.15}_{-0.14}(\text{syst})$ as reported by the CMS collaboration [65]. In this work, we focus on the result from CMS because of the rather larger error bar in the one from the ATLAS collaboration [66].

JHEP08(2021)073

- **$H_0 \to \gamma\gamma$.**
  The VLML $\psi^\pm$ can also contribute $H_0 \to \gamma\gamma$ and further reduce the SM prediction. The partial decay width of $H_0 \to \gamma\gamma$ in our model is

$$\Gamma(H_0 \to \gamma\gamma) = \frac{\alpha_{em}^2 M_{H_0}^3}{256\pi^3 v^2} \left| c_\alpha \left(I_{H_0}^f(\tau_f) + I_{H_0}^W(\tau_W) \right) + s_\alpha I_{H_0}^\psi(\tau_\psi) \right|^2 \tag{3.7}$$

  where

$$\begin{aligned} I_{H_0}^f(\tau_f) &= -2N_{cf} e_f^2 \tau_f \left[1 + (1-\tau_f) f(\tau_f)\right] \\ I_{H_0}^W(\tau_W) &= 2 + 3\tau_W + 3\tau_W(2-\tau_W) f(\tau_W) \\ I_{H_0}^\psi(\tau_\psi) &= -e_\psi^2 \frac{4y}{g} \frac{m_W}{M_\psi} \tau_\psi f(\tau_\psi) \end{aligned} \tag{3.8}$$

  with $\tau_i = 4m_i^2/M_{H_0}^2$ and

$$f(\tau) = \begin{cases} \left(\sin^{-1}\sqrt{1/\tau}\right)^2, & \tau \geq 1 \\ -\frac{1}{4}\left[\ln\left(\frac{1+\sqrt{1-\tau}}{1-\sqrt{1-\tau}}\right) - i\pi\right]^2, & \tau < 1 \end{cases} \tag{3.9}$$

  where α_{em} is the fine-structure constant and $N_c = 3(1)$ for quarks (charged leptons). We require the measured signal strength of $H_0 \to \gamma\gamma$, relative to the SM prediction, to be $1.12^{+0.07}_{-0.06}(\text{stat})^{+0.06}_{-0.07}(\text{syst})$ from CMS collaboration [67].

3.2 The LEP and LHC A_0 searches

The pseudoscalar A_0 with a mass of 52 GeV can be explored at the LEP and LHC experiments. The decay modes of A_0 for these searches are $A_0 \to b\bar{b}, \tau^+\tau^-, \mu^+\mu^-$. For the search at LEP, the most stringent limit is $\sin^2\alpha \times \text{BR}(A_0 \to b\bar{b}) \lesssim 3.5 \times 10^{-2}$ from the $e^+e^- \to ZA_0$ production [68]. On the other hand, the multilepton final states from the LHC search $pp \to t\bar{t}\,(A_0 \to \mu^+\mu^-)$ can provide a strong constraint on $\sin^2\alpha \times \text{BR}(A_0 \to \mu^+\mu^-) \lesssim 5 \times 10^{-3}$ [69]. Finally, our model is unconstrained in the $A_0 \to \tau^+\tau^-$ channel where A_0 is produced via $pp \to b\bar{b}A_0$ [70]. We will see in section 4 that the allowed range for $\sin\alpha$ remains smaller than these A_0 limits from LEP and LHC.

3.3 The DM phenomenology

The DM phenomenology can be classified in three parts:

- **DM relic density.**
  Since we fixed the mass of A_0 to be $M_{A_0} = 52$ GeV and the annihilation channel $\chi\overline{\chi} \to \psi^+\psi^-$ is kinematically forbidden, one would expect that the Higgs resonance regions $\chi\overline{\chi} \to f\overline{f}$ can play an important role to enhance the annihilation cross section in the early universe. However, the Higgs exchange is suppressed by $\sin\alpha$ when compared with A_0 exchange and the dominant channel contributing to the relic density is $\chi\overline{\chi} \to \mu^\pm\psi^\mp$ via A_0 exchange when it is open. The most favorable size of $g_\chi\kappa'$ in eq. (2.7) can be determined using Planck's relic density measurement $\Omega_\chi h^2 = 0.12 \pm 0.001$ [71]. For example, a value of $\kappa' \simeq 2.46$ with $g_\chi \simeq 0.13$ can fulfill the Planck constraint for m_χ around 200 GeV.

JHEP08(2021)073

- **DM direct detection.**
  In eq. (2.5), DM interacts with quarks via H_0/A_0 exchange resulting in a suppressed tree-level amplitude for DM-nucleon elastic scattering due to small momentum transfer. With a simple estimation based on refs. [74, 75], we find that the loop contribution with the condition $g_\chi \sin\alpha \lesssim 0.05$ is still below the neutrino floor. Our upper limit $g_\chi \sin\alpha \lesssim 0.6$ could bring the loop contribution above the neutrino floor but is still well below the current XENON1T limit [1]. Note that the complete two-loop DM-nucleon elastic scattering can be found in ref. [76]. Our model corresponds to the special case with CP phases $\phi_\chi = \pi/2$ and $\phi_{\rm SM} = 0$ in eq. (2.1) of the aforementioned reference. They have shown that the full two-loop calculation can lead to a smaller cross section than previous approaches [74, 75]. As we will see in section 4, our actual result may be below $g_\chi \sin\alpha = 0.05$. Hence, we simply ignore DM direct detection constraints in this study.

- **DM indirect detection.**
  The dominant channel of DM annihilation in the present universe within our explored parameter space is still $\chi\overline{\chi} \to \mu^\pm\psi^\mp$ which is s-wave annihilation. The VLML $\psi^\mp$ can successively decay to $\mu^\mp b\bar{b}$. The final state $\mu^+\mu^- b\bar{b}$ can produce a soft photon or electron spectrum. Therefore, one may indirectly detect DM annihilation by using dSphs gamma ray data from Fermi [77] and electron-positron data from AMS02 [85]. In addition, the produced photons and relativistic electrons may ionize and heat the universe gas at the recombination epoch. Thus, one may constrain DM annihilation cross section $\langle\sigma v\rangle$ by using Cosmic Microwave Background (CMB) anisotropy data from Planck [71]. In this study, because the cosmic ray propagation is rather uncertain and CMB limit is weaker than the one from Fermi dSphs gamma ray data — in our DM mass range of interest— we will only include the Fermi dSphs data in our analysis.

3.4 The ATLAS multi-lepton search

The VLML $\psi^\pm$ with $150 \leq M_\psi \leq 450\,\text{GeV}$ in our model is in a mass range that can be explored at the LHC via single and pair productions [72]. The major single production of $\psi^\pm$ is via $gg \to H_0^*/A_0^* \to \mu^\pm\psi^\mp$ process. Since the allowed value of κ is tiny, the single production from $pp \to W^{\pm *} \to \nu\psi^\pm$ and $pp \to Z^* \to \mu^\pm\psi^\mp$ are highly suppressed regarding eq. (2.8). Alternatively, the major pair production of $\psi^\pm$ is via $pp \to \gamma^*, Z^* \to \psi^+\psi^-$ process. We have checked that the pair production from $gg \to H_0^*/A_0^* \to \psi^+\psi^-$ is much smaller than the Drell-Yan type process with our parameter settings. The production cross sections of Drell-Yan type process are only dependent on M_ψ, but the single production process is a function of M_ψ, $\sin\alpha$, κ and κ'. Therefore, we fix $\sin\alpha = 0.1$, $\kappa = 5 \times 10^{-2}$ and $\kappa' = 2.0$ but vary M_ψ from 150–450 GeV to show both single and pair productions at $\sqrt{s} = 13\,\text{TeV}$ in the left panel of figure 1. Since the cross sections of pair production are much larger than single production ones, we will focus on the constraint of ATLAS multi-lepton search [73] on the pair production channel in this analysis. We remark that

JHEP08(2021)073

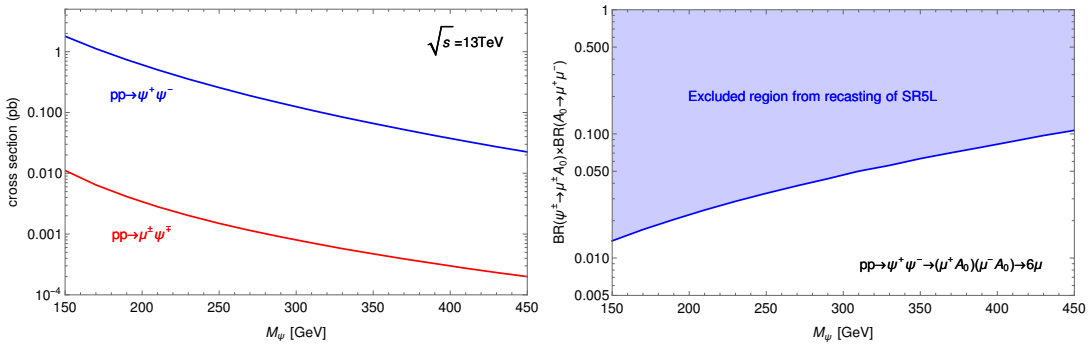

Figure 1. Left panel: the production cross sections for the VLML $\psi^{\pm}$ at $\sqrt{s} = 13\,\text{TeV}$. We fix $\sin\alpha = 0.1$, $\kappa = 5\times10^{-2}$ and $\kappa' = 2.0$ but vary M_ψ from $150-450\,\text{GeV}$. Right panel: exclusion limit from recasting of the signal region *SR5L* in [73] on $(M_\psi, BR(\psi^{\pm}\to\mu^{\pm}A_0)\times BR(A_0\to\mu^+\mu^-))$ plane.

$\psi^{\pm}\to\mu^{\pm}A_0$ is the dominant decay mode ($\text{BR}(\psi^{\pm}\to\mu^{\pm}A_0)\gtrsim 99\%$) for our parameter settings.

We closely follow the simulation and analysis in ATLAS multi-lepton search [73] based on a data sample with $\mathcal{L} = 139\,\text{fb}^{-1}$ at $\sqrt{s} = 13\,\text{TeV}$. The package `MadAnalysis 5` [78, 79] is used to recast the signal region *SR5L* for the following process

$$pp\to\gamma^*, Z^*\to\psi^+\psi^-\to(\mu^+A_0)(\mu^-A_0)\to 6\mu. \tag{3.10}$$

First, the signal processes in eq. (3.10) with up to two extra partons were generated from the leading order matrix elements by using `Madgraph5 aMC@NLO` [92]. We apply Mangano's prescription (MLM) [80, 81] for jet-parton matching with $M_\psi/4$ as the matching scale.[3] The `Pythia8` [82] is used for parton showering and merging as well as hadronization. We have modified the ATLAS template in `Delphes3` [83] to be consistent with the setup of ref. [73] for fast detector simulation. The event selections in this analysis are summarized below:

- First, in order to suppress background muons from semileptonic decays of c- and b-hadrons, any muon within $\Delta R = 0.4$ of a jet is removed.
- One of the following triggers with efficiency $\geq 90\%$ is used: (1) $P_T(\mu_1) > 27\,\text{GeV}$, (2) $P_T(\mu_{1,2}) > 15\,\text{GeV}$ and (3) $P_T(\mu_1) > 23\,\text{GeV}$, $P_T(\mu_2) > 9\,\text{GeV}$ where the subscript of muon is in the order of P_T.
- The signal muons must have $N(\mu)\geq 5$ with $P_T(\mu) > 5\,\text{GeV}$ and $|\eta(\mu)| < 2.7$.
- b-jet veto
- hadronic τ veto

[3] The K-factor (QCD corrections) for Drell-Yan type process ranges between 1.2 and 1.5. Since its effect is mild, we will not include this K-factor in our recasting.

JHEP08(2021)073

- Furthermore, to suppress low-mass particle decays from backgrounds, $m_{\mu^+\mu^-} > 4\,\text{GeV}$ and $8.4 < m_{\mu^+\mu^-} < 10.4\,\text{GeV}$ veto are required.
- Finally, if two muons are found in $\Delta R = 0.6$ and $P_T(\mu) < 30\,\text{GeV}$ for one of them, both muons are discarded. This selection is used to suppress leptons from a decay chain with multiple heavy flavour quarks backgrounds.

The model-independent limit is reported as $\langle \epsilon\sigma \rangle^{95}_{\text{obs}} = 0.129\,\text{fb}$ as calculated at 95% C.L. from the signal region *SR5L*.[4] We apply this limit to constrain $\text{BR}(\psi^\pm \to \mu^\pm A_0) \times \text{BR}(A_0 \to \mu^+\mu^-)$ for varying M_ψ as shown in the right panel of figure 1. It is expected to find that $\text{BR}(A_0 \to \mu^+\mu^-)$ already suffers from strong constraints such that A_0 cannot be muonphilic.

3.5 The EDM of electron and muon

On the EDM side, the latest electron EDM measurement from the ACME collaboration is reported as $|d_e^E| < 1.1 \times 10^{-29}\,e\,\text{cm}$ at 90% C.L. [86]. In the case of the muon EDM, the measurement from the Muon $g-2$ collaboration is $|d_\mu^E| < 1.9 \times 10^{-19}\,e\,\text{cm}$ at 95% C.L. [87]. The detailed formulas for both electron and muon EDMs in this model are given in appendix A. We adopt both electron and muon EDMs constraints in our analysis. Note that the constraints from tau and neutron EDMs from the Belle collaboration [88] and ref. [89], respectively, are much weaker than electron and muon EDM measurements in this model and can be safely ignored.

4 Results

In this section we will present our numerical results. In eq. (2.10), we show our prior ranges for the model parameters while in section 3 all the observables that are used in our analysis are discussed. The corresponding model file required for DM phenomenology is generated with `FeynRules` [90]. The DM relic density, annihilation cross section, and Higgs decay width at tree-level are computed by using `micrOMEGAs` [91]. We perform our global scan with the Markov Chain Monte Carlo package `emcee` [93].

To determine the allowed parameter space at 1σ and 2σ we analyse the data obtained via `emcee` using the profile likelihood (PL) method. This approach allows us to remove the unwanted parameters as nuisance parameters by maximizing the likelihood over them. After profiling the unwanted parameters we are left with the likelihood of the parameters we are interested in. The likelihood for n parameters of interest, $\mathcal{L}(x_1, x_2, \ldots, x_n)$, can be integrated as

$$\frac{1}{\mathcal{N}} \int_{\mathcal{C}} \mathcal{L}(x_1, x_2, \ldots, x_n) dx_1 dx_2 \ldots dx_n = \varrho \tag{4.1}$$

where $\mathcal{C}$ is the smallest n-volume with probability ϱ, x_k are placeholder parameters and $1/\mathcal{N}$ is a normalization factor with $\mathcal{N}$ the result of integrating $\mathcal{L}$ inside $\mathcal{C} \to \infty$.

[4] As pointed out in [73], there is an excess over the SM background in the signal region *SR5L* with the local significance 1.9σ. Similar to [84], our model can also explain this mild excess if it is confirmed in the future.

JHEP08(2021)073

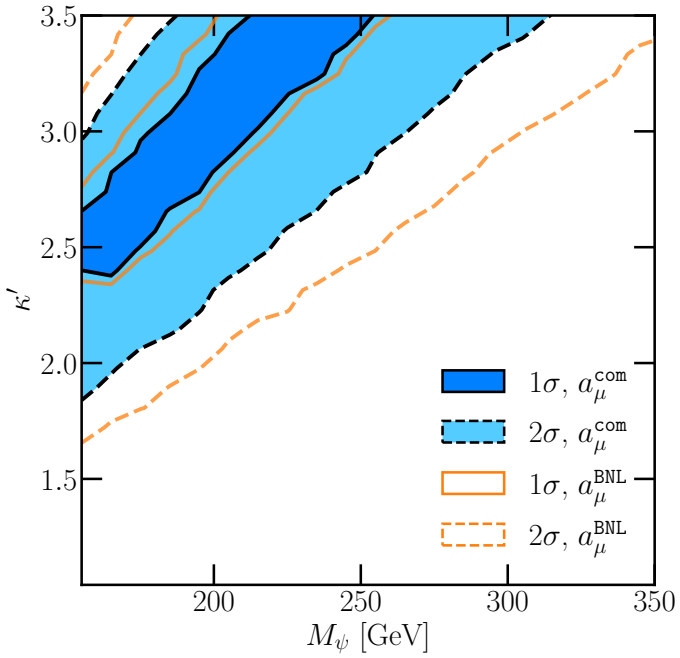

Figure 2. The VLML mass M_ψ vs. κ'. The inner and outer contours are 1σ (solid) and 2σ (dashed) confidence limits, respectively. The orange unfilled and blue filled contours correspond to the previous BNL $(g-2)_\mu$ data and the combined one from BNL and the recent E989, respectively. In addition to $(g-2)_\mu$, all the other constraints are considered.

Our likelihood function can be modeled as a pure Gaussian distribution using the total $\chi^2_{\rm total}$ in the form

$$\mathcal{L} = \exp(-\Delta\chi^2_{\rm total}/2), \qquad \Delta\chi^2_{\rm total} = \chi^2_{\rm total} - \min(\chi^2_{\rm total}). \tag{4.2}$$

In this study $\chi^2_{\rm total}$ is made with the combination of the constraints mentioned in section 3 and the appendix A:

$$\begin{aligned}\chi^2_{\rm total} = {} & \chi^2(H_0 \to A_0 A_0 \to b\bar{b}\mu^+\mu^-) + \chi^2(\Delta a_\mu) + \chi^2(\Omega h^2) \\ & + \chi^2(H_0 \text{ decays}) + \chi^2(\mu, e\text{EDM}).\end{aligned} \tag{4.3}$$

In the following subsections, we will discuss our result based on the 1σ and 2σ allowed regions of the previous BNL $(g-2)_\mu$ data (orange unfilled contours) and the combined results from BNL and the recent E989 (blue filled contours). However, all other constraints given in section 3 and appendix A are applied.

4.1 The impact from $(g-2)_\mu$ results on κ' and M_ψ

From eq. (3.2), after fixing M_{H_0} and M_{A_0}, it is easy to note that the dependence of Δa_μ is reduced to the parameters κ', M_ψ, and $\sin\alpha$. Furthermore, when compared with M_ψ and κ', smaller values of the parameter $\sin\alpha$ do not have an important effect on the value of Δa_μ due to the dominant term with $\cos\alpha$. In figure 2, we present the correlation between

JHEP08(2021)073

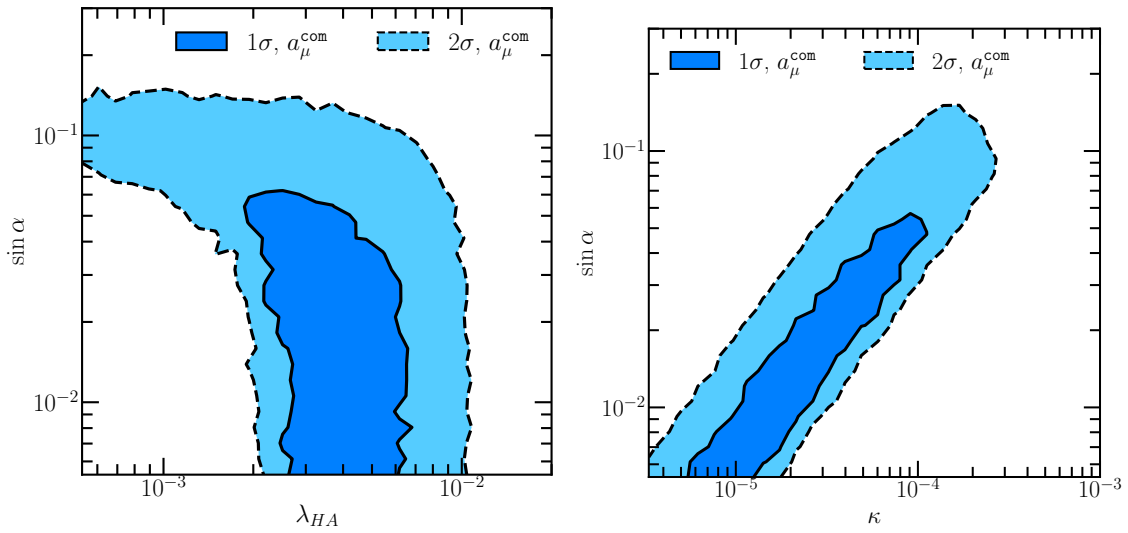

Figure 3. The likelihood distribution in the (λ_{HA}, $\sin\alpha$) plane (left) and the (κ, $\sin\alpha$) plane (right). Colors and constraints are as described in figure 2.

M_ψ and κ'. For heavier $\psi^\pm$, a larger κ' is required to satisfy the measured value of Δa_μ. It is clear that, when the new combined $(g-2)_\mu$ data is applied, the 2σ shrinks significantly while the 1σ region changes slightly. The new combined $(g-2)_\mu$ data constrains these parameters to the limits $\kappa' > 1.8$ and $M_\psi < 315\,\text{GeV}$ with an almost linearly correlation between them. In section 4.4 we will describe how these facts can help in searches for the VLML $\psi^\pm$ at the LHC.

4.2 The impact from Higgs measurements on $\sin\alpha$, λ_{HA}, and κ

In figure 3, we can clearly see that the difference between the blue and orange contours is small. As mentioned in the previous section, Δa_μ is not sensitive to $\sin\alpha$, λ_{HA}, and κ. On the other hand, the Higgs boson phenomenology is rather interesting for these three parameters. First of all, the Higgs boson exotic and invisible decay widths are functions of both $\sin\alpha$ and λ_{HA} as can be seen in eq. (3.3) and (3.5). From the left panel of figure 3 we can see the limits $\sin\alpha \lesssim 0.15$ and $\lambda_{HA} \lesssim 0.01$. Trying to be consistent with the ATLAS data for Higgs decaying to $2b2\mu$, we find that κ is proportional to $\sin\alpha$ as presented in the right panel of figure 3.

Considering that the decay width of A_0 to any fermion except the muon changes only by a constant mass factor and that all BRs add up to 1, we expect an universal relationship between $\text{BR}(A_0 \to \mu^+\mu^-)$ and $\text{BR}(A_0 \to f\bar{f})$ to be linear. The reason is that if $\text{BR}(A_0 \to b\bar{b})$ increases then $\text{BR}(A_0 \to \mu^+\mu^-)$ decreases rapidly, before $\text{BR}(A_0 \to b\bar{b})$ reaches 1. One can see, from eq. (2.6), that enhancing $\text{BR}(A_0 \to \mu^+\mu^-)$ requires larger κ, while we also need to increase $\sin\alpha$ in order to satisfy ATLAS $2b2\mu$ measurement, which depends on $\text{BR}(A_0 \to b\bar{b}) \times \text{BR}(A_0 \to \mu^+\mu^-)$.

In figure 4, we show the 2σ (dashed) and 1σ (solid) favored regions on (λ_{HA}, $\text{BR}(A_0 \to b\bar{b}) \times \text{BR}(A_0 \to \mu^+\mu^-)$) plane. When the product of both BRs is in the range 10^{-3}–4×10^{-2},

JHEP08(2021)073

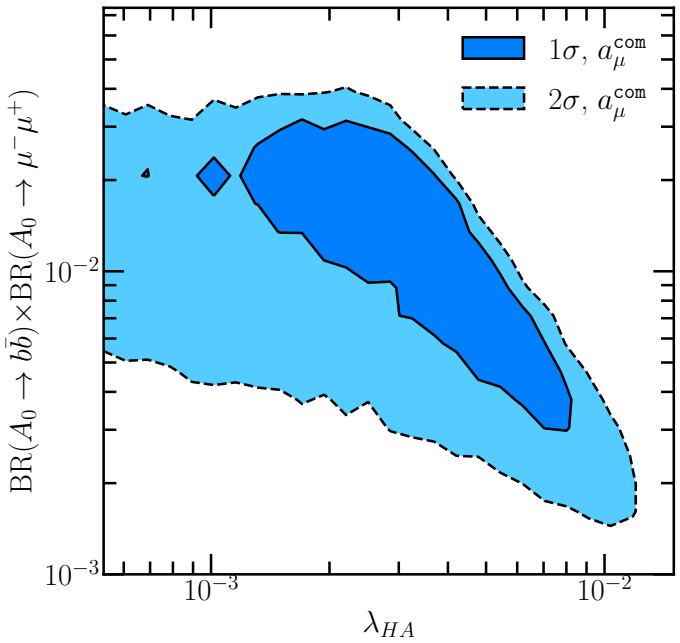

Figure 4. The two dimensional likelihood contour in the plane (λ_{HA}, $\mathrm{BR}(A_0 \to b\bar{b}) \times \mathrm{BR}(A_0 \to \mu^+\mu^-)$). Colors and constraints are as described in figure 2.

we find the limit $0.85 < \mathrm{BR}(A_0 \to b\bar{b}) < 0.89$. Finally, κ and $\sin\alpha$ are also constrained by other searches such as LHC Higgs decay ($H_0 \to \mu^+\mu^-$ and $H_0 \to \gamma\gamma$), and EDMs constraints (both electron and muon). Therefore, their values are restricted to be small as can be seen in figure 3.

4.3 The impact from DM measurements on g_χ, M_χ, M_ψ, and $\sin\alpha$

In general, the relevant model parameters for DM phenomenology are g_χ, M_χ, κ', M_ψ and $\sin\alpha$. Since the allowed range of κ' is already restricted to $1.8 < \kappa' \lesssim \sqrt{4\pi}$, here we focus on the analysis of g_χ, M_χ, M_ψ and $\sin\alpha$. In the left panel of figure 5, we can clearly observe that both ranges of M_χ and M_ψ shrink if the new measurement of $(g-2)_\mu$ is applied. Note that only $\psi^\pm$ enters to the $(g-2)_\mu$ loop calculation, but DM mass M_χ and M_ψ can be further restricted by Planck relic density constraint. In this region (larger M_χ), the dominant channel of DM annihilation is $\chi\overline{\chi} \to \mu^\pm\psi^\mp$.

For the Higgs resonance region, where the $\chi\overline{\chi} \to f\overline{f}$ is relevant, the presence of terms with $g_\chi \sin\alpha$ will bring some regions with large $g_\chi \sim \mathcal{O}(10^{-1})$ into the 2σ and 1σ regions as can be seen in the right panel of figure 5 and the g_χ column of figure 7.

In figure 6, we project the samples which agree with all the constraints and the new measurement eq. (3.1) within 2σ to (M_χ, $\langle\sigma v\rangle$) plane. The cross section of the Higgs funnel is mostly below the typical value $3 \times 10^{-26}\,\mathrm{cm}^3\,\mathrm{s}^{-1}$ because the DM velocity in the present universe becomes 10^{-3} in units of the speed of light. The resonance condition is no longer maintained. Except from the Higgs funnel, the annihilation cross section in rest of the regions is governed by $\chi\overline{\chi} \to \mu^\pm\psi^\mp$. The VLML can eventually decay to $b\bar{b}\mu^\pm$ and the

JHEP08(2021)073

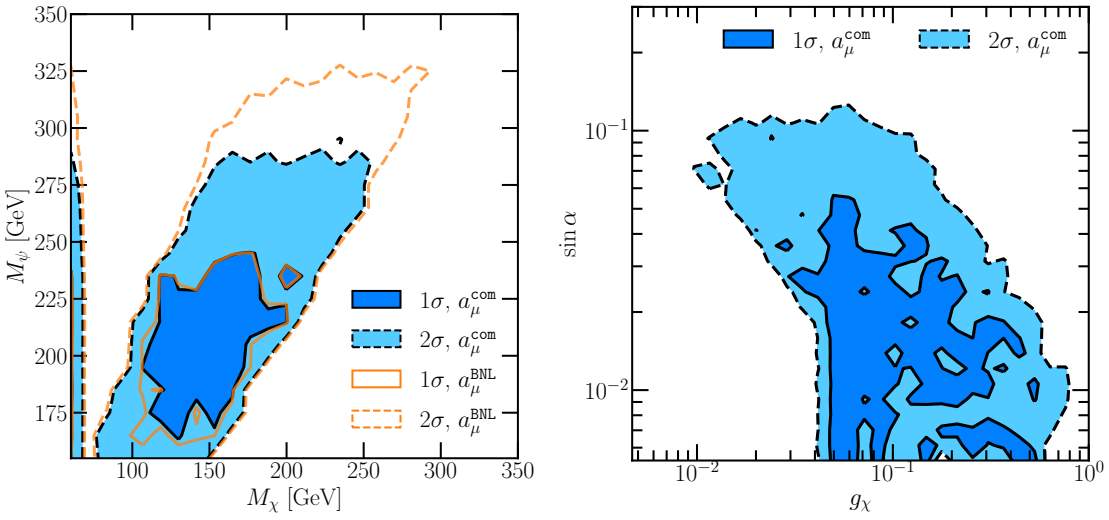

Figure 5. Likelihood distribution in the (M_χ, M_ψ) plane (left) and $(g_\chi, \sin\alpha)$ plane (right). Colors and constraints are as described in figure 2.

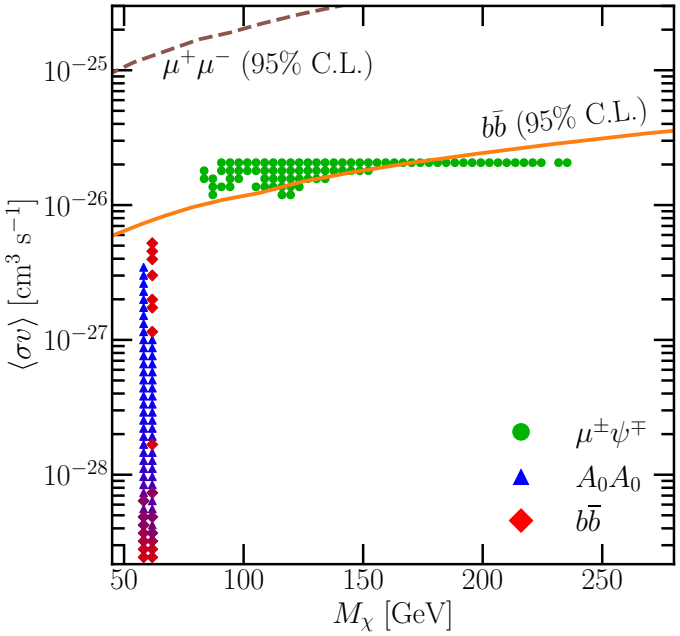

Figure 6. The 2σ allowed samples projected to $(M_\chi, \langle\sigma v\rangle)$ plane. The upper limit of dSphs gamma ray data for final state $b\bar{b}$ [99] and $\mu^+\mu^-$ [77] is depicted for reference. Different color and shape indicate the dominant DM annihilation channel.

final state of DM annihilation is $2b2\mu$. We therefore plot the 95% upper limits from dSphs gamma ray data by final states $b\bar{b}$ [99] (orange line) and $\mu^+\mu^-$ [77] (green dashed line) as comparison. At the mass range $100\,\text{GeV} \lesssim M_\chi \lesssim 200\,\text{GeV}$, the allowed parameter space may be further probed by the dSphs gamma ray data but a detailed analysis with correct gamma ray spectrum is needed.

JHEP08(2021)073

4.4 LHC

Before the end of this section, we comment some possible searches of this model at the LHC. Besides the Higgs boson invisible decay when $M_\chi < M_{H_0}/2$, a DM pair final state can be explored through mono-X processes via the off-shell exchange of H_0, A_0 [94]. In this model, the cross sections for mono-X processes are proportional to $\sin 2\alpha$, making this exploration channel a challenging one at the LHC.

We then turn to the possible new spin-0 particle A_0. Since $A_0 \to b\bar{b}$ is the dominant decay mode, the search for $H_0 \to A_0 A_0 \to b\bar{b}b\bar{b}$, as shown in refs. [95, 96], is crucial to confirm or rule out the excess presented in ref. [53]. Other option is to use $pp \to Z A_0 \to (l^+l^-)(b\bar{b})$ to confirm the existence of A_0 with $M_{A_0} = 52\,\text{GeV}$. The production cross section is about $\sin^2\alpha \times 7.67$ pb. The well-known jet substructure techniques of ref. [97] can be applied to this search for $A_0 \to b\bar{b}$.

Finally, even if the model is already constrained by the search of the pair production of VLML $\psi^\pm$ with multi-lepton signature as presented in the right panel of figure 1, we can still explore multi-b jets processes at the LHC in the near future. The signature for the single production of $\psi^\pm$ is $2\mu 2b$ and the possible SM backgrounds are $t\bar{t}$, $t\bar{b}$, $b\bar{b}Z$. Thanks to the larger cross sections of the $\psi^\pm$ pair production, one can explore this channel by two signatures: $2b4\mu$ and $4b2\mu$. The possible SM backgrounds for the former one are $t\bar{t}Z$ and $b\bar{b}ZZ$ while the SM backgrounds for the later one are $t\bar{t}t\bar{t}$, $t\bar{t}b\bar{b}$, and $t\bar{t}t\bar{b}$.

5 Conclusion and discussion

The simplified DM models are common approach for DM phenomenological studies. DM and at least one mediator are two indispensable ingredients inside these models. This opens up the possibility of discovering a mediator before finding the actual DM, thus helping us narrow down the regions worth exploring and the possible interactions between DM and the SM. Motivated by a local 3.3σ deviation at $M_{A_0} = 52\,\text{GeV}$ in the $H_0 \to A_0 A_0 \to b\bar{b}\mu^+\mu^-$ search at ATLAS Run 2, we proposed a model that this spin-0 particle A_0 is a pseudoscalar mediator. Moreover, recently the Muon $g-2$ collaboration at Fermilab hinted at BSM physics with a reported 4.2σ deviation from the SM in the combined $(g-2)_\mu$ measurements. We found that a new vector-like muon lepton (VLML) can explain both ATLAS Higgs boson exotic decay excess and $(g-2)_\mu$. In this renormalizable DM model, we involve a Dirac fermion χ and a pseudoscalar A, both SM singlets, plus an extra VLML $\psi^\pm$.

We comprehensively constrain the parameter space from this model using LHC Higgs boson data, DM measurements and electron and muon EDMs. We found that due to the close relationship between κ', $M_{\psi^\pm}$ and $(g-2)_\mu$ these parameters are bounded as $\kappa' > 1.8$ and $M_\psi < 315\,\text{GeV}$ at 2σ. Both $\sin\alpha$ and λ_{HA} are strongly affected by limits on Higgs boson exotic and invisible decays resulting in the upper bounds $\sin\alpha \lesssim 0.15$ and $\lambda_{HA} \lesssim 0.01$. To have a prediction consistent with $\text{BR}(H_0 \to A_0 A_0 \to b\bar{b}\mu^+\mu^-) \sim 3.5 \times 10^{-4}$ from ATLAS data, we found that κ is positively correlated with $\sin\alpha$ as shown in figure 3. We determined the limit to which we can enhance $\text{BR}(A_0 \to \mu^+\mu^-)$ with larger κ considering that we need to increase $\sin\alpha$ as well to satisfy $10^{-3} < \text{BR}(A_0 \to b\bar{b}) \times \text{BR}(A_0 \to \mu^+\mu^-) < 4 \times 10^{-2}$. Note that κ and $\sin\alpha$ are also constrained by $H_0 \to \mu^+\mu^-$, $H_0 \to \gamma\gamma$ and electron

JHEP08(2021)073

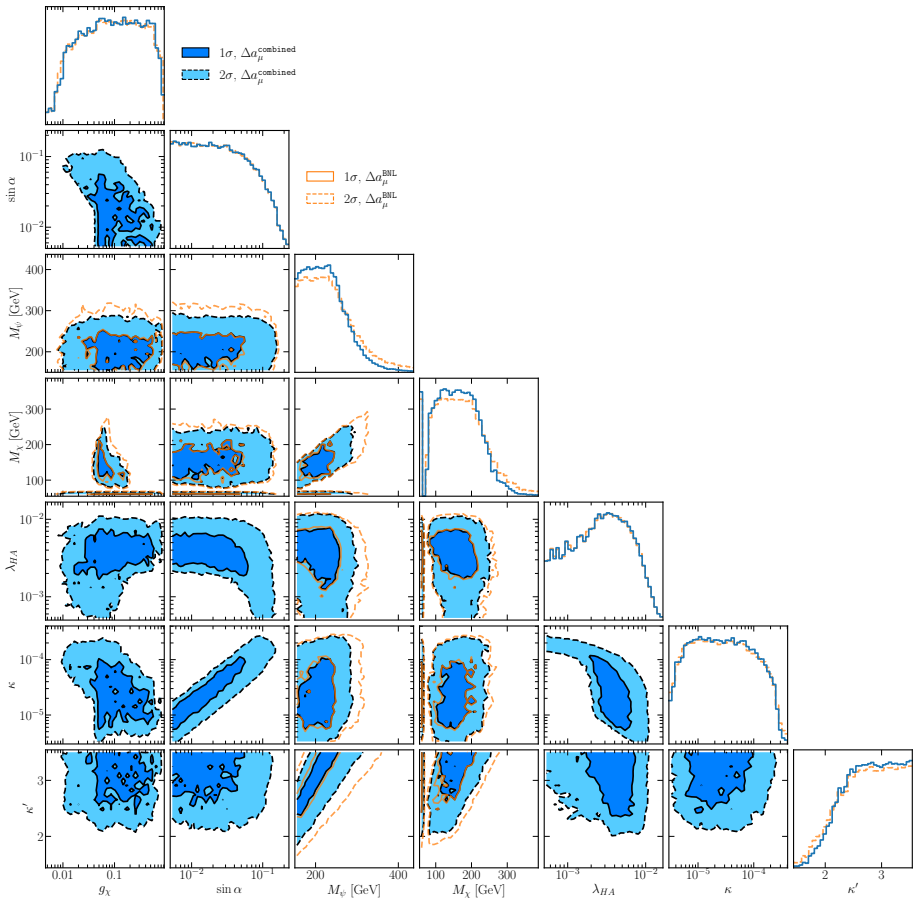

Figure 7. The likelihood distribution among seven scan parameters: g_χ, $\sin\alpha$, M_ψ, M_χ, λ_{HA}, κ, κ' in our global analysis. The 1σ and 2σ contours corresponding to using the $(g-2)_\mu$ from the E821 experiment at BNL are shown in orange, only when the change is noticeable.

and muon EDMs measurements, therefore, their values are quite restricted. In addition to the Higgs mediated resonance regions $\chi\overline{\chi} \to f\overline{f}$, the major DM annihilation channels in our model are $\chi\overline{\chi} \to \mu^\pm\psi^\mp$ via H_0/A_0 exchanges and $\chi\overline{\chi} \to H_0A_0$. Thanks to the pseudoscalar mediator, the constraints from DM direct detection can be safely ignored.

In summary, the renormalizable simplified DM model presented here simultaneously explains the ATLAS Higgs boson exotic decay excess and the recently reported $(g-2)_\mu$ result. We summarize the 1, 2 and 3σ allowed regions of all the model parameters in the triangle plot figure 7. Moreover, we have proposed ways to further confirm the existence of A_0 with a mass $M_{A_0} = 52\,\text{GeV}$ and searches for VLML $\psi^\pm$ at the LHC. Additionally, DM annihilation to $2\mu 2b$ is an interesting signature for indirect detection. Here, the first muon is primary produced but the second muon together with a pair of b-quarks come from VLML decay. The raised either electron or gamma ray spectra can be very different with the conventional DM annihilation scenario whose two final state particles carry the same energy. We will return to this in a future work.

JHEP08(2021)073

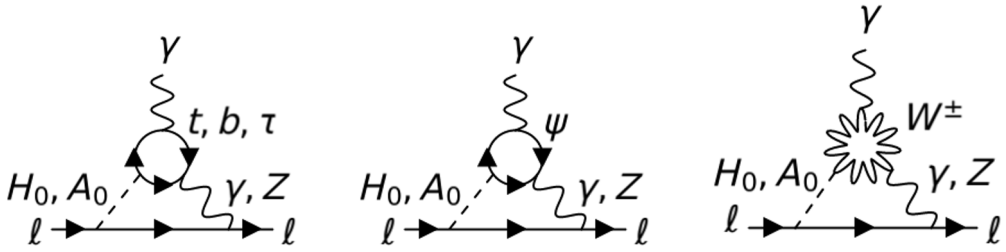

Figure 8. Two-loop Barr-Zee-type diagrams for electron and muon EDMs in our model. Note that only the diagram in the middle contributes to electron EDM.

Acknowledgments

The analysis presented here was done using the resources of the high-performance T3 Cluster at the Institute of Physics, Academia Sinica. This work is supported in part by KIAS Individual Grant, No. PG075301 (CTL) at Korea Institute for Advanced Study. Y.-L.S. Tsai was funded by the Ministry of Science and Technology Taiwan under Grant No. 109-2112-M-007-022-MY3. The work of R. Ramos is supported by the Ministry of Science and Technology of Taiwan under Grant No. 108-2811-M-001-550.

A Electron and muon electric dipole moments

In this appendix, we develop the contributions to electron and muon EDMs in our model. The effective Lagrangian for the lepton l EDM can be written as

$$\mathcal{L}^{l}_{\rm EDM} = -\frac{i}{2} d^E_l F^{\mu\nu} \bar{l} \sigma_{\mu\nu} \gamma_5 l. \tag{A.1}$$

From the interactions in eq. (2.5), we determine the explicit contributions from two-loop Barr-Zee type diagrams [100–102] for both electron and muon EDMs and display the resulting expressions in what follows.

A.1 Two-loop Barr-Zee EDMs

The electron EDM can be calculated from the two-loop Barr-Zee type diagram in the middle of figure 8. The result can be written as

$$d^E_e = (d^E_e)^{\gamma H_0/A_0} + (d^E_e)^{Z H_0/A_0} \tag{A.2}$$

where

$$\left(\frac{d^E_e}{e}\right)^{\gamma H_0/A_0} = \pm \frac{\alpha^2_{em} m_e}{8\pi^2 s^2_W m_W M_\psi} \sin 2\alpha \frac{y}{g} g_{\rm loop}(\tau_{\psi H_0/A_0}) \tag{A.3}$$

and

$$\left(\frac{d^E_e}{e}\right)^{Z H_0/A_0} = \pm \frac{\alpha^2_{em} m_e M_\psi \left(-\frac{1}{4} + s^2_W\right)}{32\pi^2 c^2_W s^2_W m_W M^2_{H_0/A_0}} \sin 2\alpha \frac{y}{g} \int_0^1 dx \frac{1}{x} J\left(\tau_{Z H_0/A_0}, \frac{\tau_{\psi H_0/A_0}}{x(1-x)}\right) \tag{A.4}$$

JHEP08(2021)073

with $\tau_{xy} = M_x^2/M_y^2$. The notation H_0/A_0 denotes summation of the contributions from H_0 and A_0 with the upper (lower) overall sign for $H_0(A_0)$.

Similarly, the muon EDM from all the two-loop Barr-Zee type diagrams in figure 8 can be written as

$$d_\mu^E = (d_\mu^E)^{\gamma H_0/A_0} + (d_\mu^E)^{Z H_0/A_0} \tag{A.5}$$

where

$$\begin{aligned}\left(\frac{d_\mu^E}{e}\right)^{\gamma H_0/A_0} =& \pm \sum_{q=t,b} \frac{3\alpha_{em}^2 Q_q^2}{4\sqrt{2}\pi^2 s_W^2 M_\psi} \sin 2\alpha \frac{\kappa'\kappa}{g^2} f_{\rm loop}(\tau_{qH_0/A_0}) \\ &\pm \frac{\alpha_{em}^2}{4\sqrt{2}\pi^2 s_W^2 M_\psi} \sin 2\alpha \frac{\kappa'\kappa}{g^2} f_{\rm loop}(\tau_{\tau H_0/A_0}) \\ &\pm \frac{\alpha_{em}^2 m_\mu}{8\pi^2 s_W^2 m_W M_\psi} \sin 2\alpha \frac{y}{g} g_{\rm loop}(\tau_{\psi H_0/A_0}) \\ &\mp \frac{\alpha_{em}^2}{16\sqrt{2}\pi^2 s_W^2 M_\psi} \sin 2\alpha \frac{\kappa'\kappa}{g^2} \mathcal{J}_W^\gamma(M_{H_0/A_0})\end{aligned} \tag{A.6}$$

and

$$\begin{aligned}\left(\frac{d_\mu^E}{e}\right)^{Z H_0/A_0} =& \pm \frac{\alpha_{em}^2 m_t^2 \left(-\frac{1}{4}+s_W^2\right)\left(\frac{1}{4}-\frac{2}{3}s_W^2\right)}{32\sqrt{2}\pi^2 c_W^2 s_W^4 M_\psi M_{H_0/A_0}^2} \sin 2\alpha \frac{\kappa'\kappa}{g^2} \int_0^1 dx \frac{1-x}{x} J\left(\tau_{Z H_0/A_0}, \frac{\tau_{tH_0/A_0}}{x(1-x)}\right) \\ &\mp \frac{\alpha_{em}^2 m_b^2 \left(-\frac{1}{4}+s_W^2\right)\left(-\frac{1}{4}+\frac{1}{3}s_W^2\right)}{64\sqrt{2}\pi^2 c_W^2 s_W^4 M_\psi M_{H_0/A_0}^2} \sin 2\alpha \frac{\kappa'\kappa}{g^2} \int_0^1 dx \frac{1-x}{x} J\left(\tau_{Z H_0/A_0}, \frac{\tau_{bH_0/A_0}}{x(1-x)}\right) \\ &\mp \frac{\alpha_{em}^2 m_\tau^2 \left(-\frac{1}{4}+s_W^2\right)^2}{64\sqrt{2}\pi^2 c_W^2 s_W^4 M_\psi M_{H_0/A_0}^2} \sin 2\alpha \frac{\kappa'\kappa}{g^2} \int_0^1 dx \frac{1-x}{x} J\left(\tau_{Z H_0/A_0}, \frac{\tau_{\tau H_0/A_0}}{x(1-x)}\right) \\ &\pm \frac{\alpha_{em}^2 m_\mu M_\psi \left(-\frac{1}{4}+s_W^2\right)}{32\pi^2 c_W^2 s_W^2 m_W M_{H_0/A_0}^2} \sin 2\alpha \frac{y}{g} \int_0^1 dx \frac{1}{x} J\left(\tau_{Z H_0/A_0}, \frac{\tau_{\psi H_0/A_0}}{x(1-x)}\right) \\ &\pm \frac{\alpha_{em}^2 \left(-\frac{1}{4}+s_W^2\right)}{16\sqrt{2}\pi^2 s_W^4 M_\psi} \sin 2\alpha \frac{\kappa'\kappa}{g^2} \mathcal{J}_W^Z(M_{H_0/A_0})\end{aligned} \tag{A.7}$$

Again, the upper (lower) overall sign is for $H_0(A_0)$. The loop functions $f_{\rm loop}(\tau)$, $g_{\rm loop}(\tau)$, $\mathcal{J}_W^{G=\gamma,Z}(M_i)$, and $J(a,b)$ can be found in refs. [100, 103, 104].

References

[1] XENON collaboration, *Dark Matter Search Results from a One Ton-Year Exposure of XENON1T*, *Phys. Rev. Lett.* **121** (2018) 111302 [arXiv:1805.12562] [INSPIRE].

[2] MUON $g-2$ collaboration, *Measurement of the Positive Muon Anomalous Magnetic Moment to 0.46 ppm*, *Phys. Rev. Lett.* **126** (2021) 141801 [arXiv:2104.03281] [INSPIRE].

JHEP08(2021)073

[3] M. Lindner, M. Platscher and F.S. Queiroz, *A Call for New Physics: The Muon Anomalous Magnetic Moment and Lepton Flavor Violation*, *Phys. Rept.* **731** (2018) 1 [arXiv:1610.06587] [INSPIRE].

[4] W. Yin and W. Yin, *Radiative lepton mass and muon $g-2$ with suppressed lepton flavor and CP-violations*, arXiv:2103.14234 [INSPIRE].

[5] C.-W. Chiang and K. Yagyu, *Radiative Seesaw Mechanism for Charged Leptons*, *Phys. Rev. D* **103** (2021) L111302 [arXiv:2104.00890] [INSPIRE].

[6] H.M. Lee, *Leptoquark option for B-meson anomalies and leptonic signatures*, *Phys. Rev. D* **104** (2021) 015007 [arXiv:2104.02982] [INSPIRE].

[7] A. Crivellin and M. Hoferichter, *Consequences of chirally enhanced explanations of $(g-2)_\mu$ for $h \to \mu\mu$ and $Z \to \mu\mu$*, *JHEP* **07** (2021) 135 [arXiv:2104.03202] [INSPIRE].

[8] M. Endo, K. Hamaguchi, S. Iwamoto and T. Kitahara, *Supersymmetric interpretation of the muon $g-2$ anomaly*, *JHEP* **07** (2021) 075 [arXiv:2104.03217] [INSPIRE].

[9] S. Iwamoto, T.T. Yanagida and N. Yokozaki, *Wino-Higgsino dark matter in the MSSM from the $g-2$ anomaly*, arXiv:2104.03223 [INSPIRE].

[10] X.-F. Han, T. Li, H.-X. Wang, L. Wang and Y. Zhang, *Lepton-specific inert two-Higgs-doublet model confronted with the new results for muon and electron $g-2$ anomalies and multi-lepton searches at the LHC*, arXiv:2104.03227 [INSPIRE].

[11] G. Arcadi, L. Calibbi, M. Fedele and F. Mescia, *Muon $g-2$ and B-anomalies from Dark Matter*, arXiv:2104.03228 [INSPIRE].

[12] J.C. Criado, A. Djouadi, N. Koivunen, K. Müürsepp, M. Raidal and H. Veermäe, *Confronting spin-3/2 and other new fermions with the muon $g-2$ measurement*, *Phys. Lett. B* **820** (2021) 136491 [arXiv:2104.03231] [INSPIRE].

[13] B. Zhu and X. Liu, *Probing the flavor-specific scalar mediator for the muon $(g-2)$ deviation, the proton radius puzzle and the light dark matter production*, arXiv:2104.03238 [INSPIRE].

[14] Y. Gu, N. Liu, L. Su and D. Wang, *Heavy bino and slepton for muon $g-2$ anomaly*, *Nucl. Phys. B* **969** (2021) 115481 [arXiv:2104.03239] [INSPIRE].

[15] H.-X. Wang, L. Wang and Y. Zhang, *muon $g-2$ anomaly and μ-τ-philic Higgs doublet with a light CP-even component*, arXiv:2104.03242 [INSPIRE].

[16] M. Van Beekveld, W. Beenakker, M. Schutten and J. De Wit, *Dark matter, fine-tuning and $(g-2)_\mu$ in the pMSSM*, arXiv:2104.03245 [INSPIRE].

[17] T. Nomura and H. Okada, *Explanations for anomalies of muon anomalous magnetic dipole moment, $b \to s\mu\bar{\mu}$ and radiative neutrino masses in a leptoquark model*, arXiv:2104.03248 [INSPIRE].

[18] D. Anselmi et al., *A fake doublet solution to the muon anomalous magnetic moment*, arXiv:2104.03249 [INSPIRE].

[19] W. Yin, *Muon $g-2$ anomaly in anomaly mediation*, *JHEP* **06** (2021) 029 [arXiv:2104.03259] [INSPIRE].

[20] F. Wang, L. Wu, Y. Xiao, J.M. Yang and Y. Zhang, *GUT-scale constrained SUSY in light of new muon $g-2$ measurement*, *Nucl. Phys. B* **970** (2021) 115486 [arXiv:2104.03262] [INSPIRE].

JHEP08(2021)073

[21] M.A. Buen-Abad, J. Fan, M. Reece and C. Sun, *Challenges for an axion explanation of the muon $g-2$ measurement*, arXiv:2104.03267 [INSPIRE].

[22] P. Das, M.K. Das and N. Khan, *The FIMP-WIMP dark matter and Muon $g-2$ in the extended singlet scalar model*, arXiv:2104.03271 [INSPIRE].

[23] M. Abdughani, Y.-Z. Fan, L. Feng, Y.-L.S. Tsai, L. Wu and Q. Yuan, *A common origin of muon $g-2$ anomaly, Galaxy Center GeV excess and AMS-02 anti-proton excess in the NMSSM*, arXiv:2104.03274 [INSPIRE].

[24] C.-H. Chen, C.-W. Chiang and T. Nomura, *Muon $g-2$ in two-Higgs-doublet model with type-II seesaw mechanism*, arXiv:2104.03275 [INSPIRE].

[25] S.-F. Ge, X.-D. Ma and P. Pasquini, *Probing the Dark Axion Portal with Muon Anomalous Magnetic Moment*, arXiv:2104.03276 [INSPIRE].

[26] M. Cadeddu, N. Cargioli, F. Dordei, C. Giunti and E. Picciau, *Muon and electron $g-2$ and proton and cesium weak charges implications on dark Z_d models*, *Phys. Rev. D* **104** (2021) L011701 [arXiv:2104.03280] [INSPIRE].

[27] V. Brdar, S. Jana, J. Kubo and M. Lindner, *Semi-secretly interacting Axion-like particle as an explanation of Fermilab muon $g-2$ measurement*, *Phys. Lett. B* **820** (2021) 136529 [arXiv:2104.03282] [INSPIRE].

[28] J. Cao, J. Lian, Y. Pan, D. Zhang and P. Zhu, *Improved $(g-2)_\mu$ Measurement and Singlino dark matter in the general NMSSM*, arXiv:2104.03284 [INSPIRE].

[29] M. Chakraborti, S. Heinemeyer and I. Saha, *The new "MUON G-2" Result and Supersymmetry*, arXiv:2104.03287 [INSPIRE].

[30] M. Ibe, S. Kobayashi, Y. Nakayama and S. Shirai, *Muon $g-2$ in Gauge Mediation without SUSY CP Problem*, arXiv:2104.03289 [INSPIRE].

[31] P. Cox, C. Han and T.T. Yanagida, *Muon $g-2$ and Co-annihilating Dark Matter in the MSSM*, arXiv:2104.03290 [INSPIRE].

[32] K.S. Babu, S. Jana, M. Lindner and P.K. Vishnu, *Muon $g-2$ Anomaly and Neutrino Magnetic Moments*, arXiv:2104.03291 [INSPIRE].

[33] C. Han, *Muon $g-2$ and CP-violation in MSSM*, arXiv:2104.03292 [INSPIRE].

[34] S. Heinemeyer, E. Kpatcha, I. Lara, D.E. López-Fogliani, C. Muñoz and N. Nagata, *The new $(g-2)_\mu$ result and the $\mu\nu$SSM*, arXiv:2104.03294 [INSPIRE].

[35] L. Calibbi, M.L. López-Ibáñez, A. Melis and O. Vives, *Implications of the Muon $g-2$ result on the flavour structure of the lepton mass matrix*, arXiv:2104.03296 [INSPIRE].

[36] D.W.P. Amaral, D.G. Cerdeño, A. Cheek and P. Foldenauer, *Distinguishing $\mathrm{U}(1)_{L_\mu - L_\tau}$ from $\mathrm{U}(1)_{L_\mu}$ as a solution for $(g-2)_\mu$ with neutrinos*, arXiv:2104.03297 [INSPIRE].

[37] Y. Bai and J. Berger, *Muon $g-2$ in Lepton Portal Dark Matter*, arXiv:2104.03301 [INSPIRE].

[38] S. Baum, M. Carena, N.R. Shah and C.E.M. Wagner, *The Tiny $(g-2)$ Muon Wobble from Small-μ Supersymmetry*, arXiv:2104.03302 [INSPIRE].

[39] T. Li, J. Pei and W. Zhang, *Muon Anomalous Magnetic Moment and Higgs Potential Stability in the 331 Model from E_6*, arXiv:2104.03334 [INSPIRE].

JHEP08(2021)073

[40] L. Zu, X. Pan, L. Feng, Q. Yuan and Y.-Z. Fan, *Constraining* $U(1)_{L_\mu - L_\tau}$ *charged dark matter model for muon* $g-2$ *anomaly with AMS-02 electron and positron data*, arXiv:2104.03340 [INSPIRE].

[41] W.-Y. Keung, D. Marfatia and P.-Y. Tseng, *Axion-like particles, two-Higgs-doublet models, leptoquarks, and the electron and muon* $g-2$, arXiv:2104.03341 [INSPIRE].

[42] P.M. Ferreira, B.L. Gonçalves, F.R. Joaquim and M. Sher, $(g-2)_\mu$ *in the 2HDM and slightly beyond — an updated view*, arXiv:2104.03367 [INSPIRE].

[43] H.-B. Zhang, C.-X. Liu, J.-L. Yang and T.-F. Feng, *Muon anomalous magnetic dipole moment in the* $\mu\nu SSM$, arXiv:2104.03489 [INSPIRE].

[44] W. Ahmed, I. Khan, J. Li, T. Li, S. Raza and W. Zhang, *The Natural Explanation of the Muon Anomalous Magnetic Moment via the Electroweak Supersymmetry from the GmSUGRA in the MSSM*, arXiv:2104.03491 [INSPIRE].

[45] R. Zhou, L. Bian and J. Shu, *Probing new physics for* $(g-2)_\mu$ *and gravitational waves*, arXiv:2104.03519 [INSPIRE].

[46] J.-L. Yang, H.-B. Zhang, C.-X. Liu, X.-X. Dong and T.-F. Feng, *Muon* $(g-2)$ *in the B-LSSM*, arXiv:2104.03542 [INSPIRE].

[47] P. Athron, C. Balázs, D.H. Jacob, W. Kotlarski, D. Stöckinger and H. Stöckinger-Kim, *New physics explanations of* a_μ *in light of the FNAL muon* $g-2$ *measurement*, arXiv:2104.03691 [INSPIRE].

[48] J. Chen, Q. Wen, F. Xu and M. Zhang, *Flavor Anomalies Accommodated in A Flavor Gauged Two Higgs Doublet Model*, arXiv:2104.03699 [INSPIRE].

[49] E.J. Chun and T. Mondal, *Leptophilic bosons and muon* $g-2$ *at lepton colliders*, *JHEP* **07** (2021) 044 [arXiv:2104.03701] [INSPIRE].

[50] P. Escribano, J. Terol-Calvo and A. Vicente, $(g-2)_{e,\mu}$ *in an extended inverse type-III seesaw model*, *Phys. Rev. D* **103** (2021) 115018 [arXiv:2104.03705] [INSPIRE].

[51] A. Aboubrahim, M. Klasen and P. Nath, *What Fermilab* $(g-2)_\mu$ *experiment tells us about discovering SUSY at HL-LHC and HE-LHC*, arXiv:2104.03839 [INSPIRE].

[52] B. Bhattacharya, A. Datta, D. Marfatia, S. Nandi and J. Waite, *Axion-like particles resolve the* $B \to \pi K$ *and* $g-2$ *anomalies*, arXiv:2104.03947 [INSPIRE].

[53] ATLAS collaboration, *Search for Higgs boson decays into two spin-0 particles in the* $bb\mu\mu$ *final state with the ATLAS detector in pp collisions at* $\sqrt{s} = 13$ *TeV*, ATLAS-CONF-2021-009 (2021) [INSPIRE].

[54] G.C. Branco, P.M. Ferreira, L. Lavoura, M.N. Rebelo, M. Sher and J.P. Silva, *Theory and phenomenology of two-Higgs-doublet models*, *Phys. Rept.* **516** (2012) 1 [arXiv:1106.0034] [INSPIRE].

[55] D. Sabatta, A.S. Cornell, A. Goyal, M. Kumar, B. Mellado and X. Ruan, *Connecting muon anomalous magnetic moment and multi-lepton anomalies at LHC*, *Chin. Phys. C* **44** (2020) 063103 [arXiv:1909.03969] [INSPIRE].

[56] D. Curtin et al., *Exotic decays of the* 125 *GeV Higgs boson*, *Phys. Rev. D* **90** (2014) 075004 [arXiv:1312.4992] [INSPIRE].

JHEP08(2021)073

[57] ATLAS collaboration, *A combination of measurements of Higgs boson production and decay using up to 139 fb^{-1} of proton-proton collision data at $\sqrt{s} = 13$ TeV collected with the ATLAS experiment*, ATLAS-CONF-2020-027 (2020) [INSPIRE].

[58] M. Davier, A. Hoecker, B. Malaescu and Z. Zhang, *A new evaluation of the hadronic vacuum polarisation contributions to the muon anomalous magnetic moment and to $\alpha(m_Z^2)$*, *Eur. Phys. J. C* **80** (2020) 241 [*Erratum ibid.* **80** (2020) 410] [arXiv:1908.00921] [INSPIRE].

[59] S. Borsányi et al., *Leading hadronic contribution to the muon magnetic moment from lattice QCD*, *Nature* **593** (2021) 51 [arXiv:2002.12347] [INSPIRE].

[60] G. Hiller, C. Hormigos-Feliu, D.F. Litim and T. Steudtner, *Anomalous magnetic moments from asymptotic safety*, *Phys. Rev. D* **102** (2020) 071901 [arXiv:1910.14062] [INSPIRE].

[61] S. Baek, P. Ko and J. Li, *Minimal renormalizable simplified dark matter model with a pseudoscalar mediator*, *Phys. Rev. D* **95** (2017) 075011 [arXiv:1701.04131] [INSPIRE].

[62] PARTICLE DATA collaboration, *Review of Particle Physics*, *Phys. Rev. D* **98** (2018) 030001 [INSPIRE].

[63] ATLAS collaboration, *Constraints on new phenomena via Higgs boson couplings and invisible decays with the ATLAS detector*, *JHEP* **11** (2015) 206 [arXiv:1509.00672] [INSPIRE].

[64] ATLAS and CMS collaborations, *Measurements of the Higgs boson production and decay rates and constraints on its couplings from a combined ATLAS and CMS analysis of the LHC pp collision data at $\sqrt{s} = 7$ and 8 TeV*, *JHEP* **08** (2016) 045 [arXiv:1606.02266] [INSPIRE].

[65] CMS collaboration, *Evidence for Higgs boson decay to a pair of muons*, *JHEP* **01** (2021) 148 [arXiv:2009.04363] [INSPIRE].

[66] ATLAS collaboration, *A search for the dimuon decay of the Standard Model Higgs boson with the ATLAS detector*, *Phys. Lett. B* **812** (2021) 135980 [arXiv:2007.07830] [INSPIRE].

[67] CMS collaboration, *Measurements of Higgs boson production cross sections and couplings in the diphoton decay channel at $\sqrt{s} = 13$ TeV*, *JHEP* **07** (2021) 027 [arXiv:2103.06956] [INSPIRE].

[68] LEP Working Group for Higgs boson searches, ALEPH, DELPHI, L3 and OPAL collaborations, *Search for the standard model Higgs boson at LEP*, *Phys. Lett. B* **565** (2003) 61 [hep-ex/0306033] [INSPIRE].

[69] CMS collaboration, *Search for new physics in multilepton final states in pp collisions at $\sqrt{s} = 13$ TeV*, CMS-PAS-EXO-19-002 (2019) [INSPIRE].

[70] CMS collaboration, *Search for a low-mass $\tau^+\tau^-$ resonance in association with a bottom quark in proton-proton collisions at $\sqrt{s} = 13$ TeV*, *JHEP* **05** (2019) 210 [arXiv:1903.10228] [INSPIRE].

[71] PLANCK collaboration, *Planck 2018 results. VI. Cosmological parameters*, *Astron. Astrophys.* **641** (2020) A6 [arXiv:1807.06209] [INSPIRE].

[72] S. Bißmann, G. Hiller, C. Hormigos-Feliu and D.F. Litim, *Multi-lepton signatures of vector-like leptons with flavor*, *Eur. Phys. J. C* **81** (2021) 101 [arXiv:2011.12964] [INSPIRE].

JHEP08(2021)073

[73] ATLAS collaboration, *Search for supersymmetry in events with four or more charged leptons in 139 fb^{-1} of $\sqrt{s} = 13$ TeV pp collisions with the ATLAS detector*, arXiv:2103.11684 [INSPIRE].

[74] G. Arcadi, M. Lindner, F.S. Queiroz, W. Rodejohann and S. Vogl, *Pseudoscalar Mediators: A WIMP model at the Neutrino Floor*, *JCAP* **03** (2018) 042 [arXiv:1711.02110] [INSPIRE].

[75] T. Abe, M. Fujiwara and J. Hisano, *Loop corrections to dark matter direct detection in a pseudoscalar mediator dark matter model*, *JHEP* **02** (2019) 028 [arXiv:1810.01039] [INSPIRE].

[76] F. Ertas and F. Kahlhoefer, *Loop-induced direct detection signatures from CP-violating scalar mediators*, *JHEP* **06** (2019) 052 [arXiv:1902.11070] [INSPIRE].

[77] FERMI-LAT collaboration, *Searching for Dark Matter Annihilation from Milky Way Dwarf Spheroidal Galaxies with Six Years of Fermi Large Area Telescope Data*, *Phys. Rev. Lett.* **115** (2015) 231301 [arXiv:1503.02641] [INSPIRE].

[78] E. Conte, B. Dumont, B. Fuks and C. Wymant, *Designing and recasting LHC analyses with MadAnalysis 5*, *Eur. Phys. J. C* **74** (2014) 3103 [arXiv:1405.3982] [INSPIRE].

[79] B. Dumont et al., *Toward a public analysis database for LHC new physics searches using MADANALYSIS 5*, *Eur. Phys. J. C* **75** (2015) 56 [arXiv:1407.3278] [INSPIRE].

[80] M.L. Mangano, M. Moretti, F. Piccinini and M. Treccani, *Matching matrix elements and shower evolution for top-quark production in hadronic collisions*, *JHEP* **01** (2007) 013 [hep-ph/0611129] [INSPIRE].

[81] J. Alwall et al., *Comparative study of various algorithms for the merging of parton showers and matrix elements in hadronic collisions*, *Eur. Phys. J. C* **53** (2008) 473 [arXiv:0706.2569] [INSPIRE].

[82] T. Sjöstrand, S. Mrenna and P.Z. Skands, *A Brief Introduction to PYTHIA 8.1*, *Comput. Phys. Commun.* **178** (2008) 852 [arXiv:0710.3820] [INSPIRE].

[83] DELPHES 3 collaboration, *DELPHES 3, A modular framework for fast simulation of a generic collider experiment*, *JHEP* **02** (2014) 057 [arXiv:1307.6346] [INSPIRE].

[84] J. Kawamura and S. Raby, *$\geq 4\mu$ signal from a vector-like lepton decaying to a muon-philic Z' boson at the LHC*, arXiv:2104.04461 [INSPIRE].

[85] AMS collaboration, *The Alpha Magnetic Spectrometer (AMS) on the international space station: Part II — Results from the first seven years*, *Phys. Rept.* **894** (2021) 1 [INSPIRE].

[86] ACME collaboration, *Improved limit on the electric dipole moment of the electron*, *Nature* **562** (2018) 355 [INSPIRE].

[87] MUON $(g-2)$ collaboration, *An Improved Limit on the Muon Electric Dipole Moment*, *Phys. Rev. D* **80** (2009) 052008 [arXiv:0811.1207] [INSPIRE].

[88] BELLE collaboration, *Search for the electric dipole moment of the tau lepton*, *Phys. Lett. B* **551** (2003) 16 [hep-ex/0210066] [INSPIRE].

[89] J.M. Pendlebury et al., *Revised experimental upper limit on the electric dipole moment of the neutron*, *Phys. Rev. D* **92** (2015) 092003 [arXiv:1509.04411] [INSPIRE].

[90] A. Alloul, N.D. Christensen, C. Degrande, C. Duhr and B. Fuks, *FeynRules 2.0 — A complete toolbox for tree-level phenomenology*, *Comput. Phys. Commun.* **185** (2014) 2250 [arXiv:1310.1921] [INSPIRE].

JHEP08(2021)073

[91] G. Bélanger, A. Mjallal and A. Pukhov, *Recasting direct detection limits within MicrOMEGAs and implication for non-standard Dark Matter scenarios*, *Eur. Phys. J. C* **81** (2021) 239 [arXiv:2003.08621] [INSPIRE].

[92] J. Alwall et al., *The automated computation of tree-level and next-to-leading order differential cross sections, and their matching to parton shower simulations*, *JHEP* **07** (2014) 079 [arXiv:1405.0301] [INSPIRE].

[93] D. Foreman-Mackey, D.W. Hogg, D. Lang and J. Goodman, *emcee: The MCMC Hammer*, *Publ. Astron. Soc. Pac.* **125** (2013) 306 [arXiv:1202.3665] [INSPIRE].

[94] F. Kahlhoefer, *Review of LHC Dark Matter Searches*, *Int. J. Mod. Phys. A* **32** (2017) 1730006 [arXiv:1702.02430] [INSPIRE].

[95] ATLAS collaboration, *Search for the Higgs boson produced in association with a vector boson and decaying into two spin-zero particles in the $H \to aa \to 4b$ channel in pp collisions at $\sqrt{s} = 13$ TeV with the ATLAS detector*, *JHEP* **10** (2018) 031 [arXiv:1806.07355] [INSPIRE].

[96] ATLAS collaboration, *Search for Higgs boson decays into two new low-mass spin-0 particles in the 4b channel with the ATLAS detector using pp collisions at $\sqrt{s} = 13$ TeV*, *Phys. Rev. D* **102** (2020) 112006 [arXiv:2005.12236] [INSPIRE].

[97] J.M. Butterworth, A.R. Davison, M. Rubin and G.P. Salam, *Jet substructure as a new Higgs search channel at the LHC*, *Phys. Rev. Lett.* **100** (2008) 242001 [arXiv:0802.2470] [INSPIRE].

[98] CMS collaboration, *Search for vector-like leptons in multilepton final states in proton-proton collisions at $\sqrt{s} = 13$ TeV*, *Phys. Rev. D* **100** (2019) 052003 [arXiv:1905.10853] [INSPIRE].

[99] Fermi-LAT, HAWC, H.E.S.S., MAGIC and VERITAS collaborations, *Combined Dark Matter searches towards dwarf spheroidal galaxies with Fermi-LAT, HAWC, HESS, MAGIC and VERITAS*, *PoS* **ICRC2019** (2021) 012 [arXiv:1909.06310] [INSPIRE].

[100] J.R. Ellis, J.S. Lee and A. Pilaftsis, *Electric Dipole Moments in the MSSM Reloaded*, *JHEP* **10** (2008) 049 [arXiv:0808.1819] [INSPIRE].

[101] G.F. Giudice and A. Romanino, *Electric dipole moments in split supersymmetry*, *Phys. Lett. B* **634** (2006) 307 [hep-ph/0510197] [INSPIRE].

[102] Y. Li, S. Profumo and M. Ramsey-Musolf, *Higgs-Higgsino-Gaugino Induced Two Loop Electric Dipole Moments*, *Phys. Rev. D* **78** (2008) 075009 [arXiv:0806.2693] [INSPIRE].

[103] J.R. Ellis, J.S. Lee and A. Pilaftsis, *A Geometric Approach to CP-violation: Applications to the MCPMFV SUSY Model*, *JHEP* **10** (2010) 049 [arXiv:1006.3087] [INSPIRE].

[104] T. Abe, J. Hisano, T. Kitahara and K. Tobioka, *Gauge invariant Barr-Zee type contributions to fermionic EDMs in the two-Higgs doublet models*, *JHEP* **01** (2014) 106 [*Erratum JHEP* **04** (2016) 161] [arXiv:1311.4704] [INSPIRE].

JHEP08(2021)073